Open Access

Journal of Energy and Power Technology

LIDSEN Publishing Inc.

Original Research

A Rechargeable Aqueous Lithium-Air Battery with an Acetic Acid Catholyte Operated at High Pressure

Syuma Ichida [1], Daisuke Mori [1], Sou Taminato [1], Tao Zhang [2], Yasuo Takeda [1], Osamu Yamamoto [1,*], Nobuyuki Imanishi [1]

1. Graduate School of Engineering, Mie University, Tsu, Mie, 514-8507, Japan; E-Mails: 420m303@m.mie-u.ac.jp; daisuke.mori@chem.mie-u.ac.jp; taminato@chem.mie-u.ac.jp; takeda@chem.mie-u.ac.jp; yamamoto@chem.mie-u.ac.jp; imanishi@chiem.mie-u.ac.jp
2. State Key Laboratory of High Performance Cermic and Super Microstructure, Shanghai Institute of Cermaics, CAS, 200050, People Republic China; E-Mail: taozhang@mail.sic.ac.cn

* **Correspondence:** Osamu Yamamoto; E-Mail: yamamoto@chem.mie-u.ac.jp

Academic Editor: Ahamed Irshad

Special Issue: Batteries: Past, Present and Future

Journal of Energy and Power Technology
2022, volume 4, issue 1
doi:10.21926/jept.2201009

Received: February 17, 2022
Accepted: March 11, 2022
Published: March 15, 2022

Abstract

Acidic aqueous lithium-air batteries are attractive candidates for use as energy sources in electric vehicles because of their high energy and power densities and ability to operate under ambient conditions. An aqueous lithium-air battery with an acetic acid catholyte has a high theoretical energy density of 1,478 Wh kg^{-1}, and the reaction product is soluble in the catholyte. In this study, we have studied the cell performance of a Li/interlayer electrolyte/NASICON-type solid lithium-ion conductor/acetic acid catholyte/air electrode cell at high pressure and room temperature under air. The cell was successfully operated at 0.5 mA cm^{-2} and 0.2 MPa.

Keywords

High energy density battery; lithium-air battery; aqueous battery, solid lithium-ion conductor; acetic acid

1. Introduction

The demand for higher energy power density rechargeable batteries for electric vehicle (EV) applications has increased [1, 2]. Many types of advanced rechargeable batteries beyond lithium-ion batteries have been proposed and developed, such as non-aqueous lithium-air [3], aqueous lithium-air [3], lithium-sulfur [4], multivalent [5], and lithium solid-state batteries [6]. The theoretical energy densities of these advanced batteries are several times higher than those of conventional lithium-ion batteries. However, these batteries have serious problems to solve before their practical use as power sources in EVs, such as the elimination of water in the air in the non-aqueous lithium-air battery, dissolution of the reaction product into the electrolyte in the lithium-sulfur battery, and poor contact between the electrolyte and cathode active materials in the solid-state battery. Of the options available, the aqueous lithium-air battery is particularly attractive for EVs because the battery has the potential for high energy and power densities, but no serious problems to be solved. The aqueous lithium-air battery consists of a lithium anode, an interlayer non-aqueous electrolyte, a water-stable lithium-ion conducting solid electrolyte, an aqueous catholyte, and an air electrode. Two types of aqueous lithium-air batteries have been developed; one contains an alkaline catholyte of LiOH [7], and the other contains an acid catholyte such as acetic acid, CH_3COOH (HAc) [8]. The cell reactions are as follows:
for alkaline catholyte

$$4\mathrm{Li} + 6\mathrm{H_2O} + \mathrm{O_2} = 4(\mathrm{LiOH \cdot H_2O}), \quad (1)$$

and for acid catholyte

$$2\mathrm{Li} + 2\mathrm{CH_3COOH} + {}^{1}\!/_{2}\,\mathrm{O_2} = 2\mathrm{CH_3COOLi} + \mathrm{H_2O}. \quad (2)$$

The theoretical energy densities of the alkaline and acid systems with HAc are 1910 and 1478 Wh kg^{-1}, respectively, which are lower than that of the non-aqueous lithium-air system at 3458 Wh kg^{-1}, but more than three times higher than that of the conventional lithium-ion battery. Alkaline type aqueous lithium-air batteries have shown susceptibility to contamination from CO_2 in the air and produced Li_2CO_3 on the air electrode surface, which resulted in degradation of the cell performance. The acid aqueous lithium-air battery (ALAB) is not susceptible to contamination from CO_2. Several types of ALAB with various catholytes such as HAc aqueous solution [9], 0.1 M H_3PO_4-LiH_2PO_4 buffer solution [10], and a 1 M $LiNO_3$ aqueous solution [11] have been proposed. The water-stable NASICON-type and perovskite lithium-ion conducting solid electrolytes are unstable in strong acid aqueous solution [12]; therefore, weak acid aqueous solutions have been used for ALAB. ALAB with an HAc aqueous solution showed the highest specific energy density among the previously reported aqueous systems. The first ALAB was operated at 60 °C because a polyethylene-based polymer electrolyte was used as the interlayer electrolyte to suppress lithium dendrite formation at the lithium electrode [8]. A room temperature ALAB with a HAc catholyte was reported using a lithium dendrite-free interlayer electrolyte by Imanishi and co-workers [9]. One of the issues of ALAB with HAc is the evaporation of the catholyte over a long operation

period. In this study, the cell performance of an ALAB at 0.2 MPa was examined with the goal of suppressing catholyte evaporation.

2. Experimental

Figure 1 shows a schematic diagram of the in-house-built Swagelok-type ALAB test cell and a high-pressure vessel. The cell consists of a 200 µm thick lithium anode (Honjyo Metal, Japan), an interlayer electrolyte of 1 M lithium bis(fluorosulfonyl)imide (LiFSI) (Central Glass, Japan) in 1,4 dioxane (DX)-1,2 dimethoxyethane (DME) (1:2 v/v), a 250 µm thick $Li_{1+x+y}Al_x(Ti, Ge)_{2-x}Si_yP_{3-y}O_{12}$ (LATP; Ohara, Japan) separator, a HAc-saturated CH_3COOLi (LiAc) aqueous solution (9:1 v/v) catholyte, and a platinum-loaded porous carbon (Pt/C; Tanaka Kikinzoku, Japan) with vapor growth carbon nanofiber (VGCF; Showa Denko, Japan) or Ketjenblack (KB; Lion Special Chemicals, Japan) mixture air electrode. The electrolyte volumes of the catholyte and anolyte were approximately 1 mL, and their thicknesses were approximately 0.9 cm. The interlayer electrolyte of 1 M LiFSI in DX-DME (1:2 v/v) was reported to be free of lithium dendrite formation at a high current density [13]. The water-impermeable NASICON-type LATP glass-ceramic is acceptable as the separator for the ALAB because it is stable in weakly acidic aqueous solution and has a high lithium-ion conductivity of around 10^{-4} S cm^{-1} at room temperature [12]. The air electrode was prepared by mixing Pt-C, VGCF (or KB), and polytetrafluoroethylene (PTFE) (Daikin, Japan) of around 0.2 mg, which was then was pressed onto a titanium mesh of 1.5 cm^2 (Nikora, Japan). A carbon paper gas diffusion layer (Toray, Japan) was attached to the air electrode.

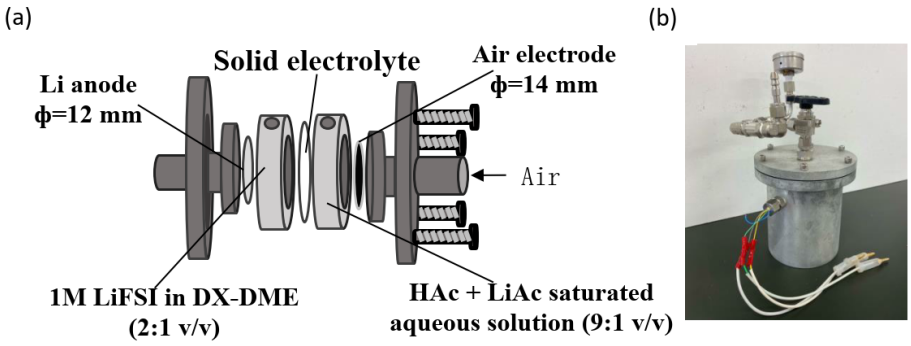

Figure 1 (a) Schematic diagram of the test cell of Li/1 M LiFSI in DX-DME (1:2 v/v)/LATP/HAc-saturated LiAc aqueous solution (9:1 v/v)/Pt/C-VGCF-PTFE, air; and (b) photograph of the high-pressure chamber.

The performance of the air electrode was measured using a half cell with the air electrode, a Pt-black counter electrode, and an Ag/AgCl reference electrode in an air atmosphere at 0.2 MPa and 25 °C. The full cell was set up using the in-house-built Swagelok-type cell. The pressure was controlled using a Swagelok return check valve, and the flow rate of air was kept at 80 mL min^{-1}, which was checked using a gas flow meter. The evaporation rate of the catholyte was estimated from the weight change with time at 0.2 and 0.1 MPa and with an airflow rate of 80 mL min^{-1}.

The electrochemical performance of the half and full cells was investigated using a battery cycler (Nagano BTS, 200H, Japan) and a multichannel potentio/galvanostat (Bio-Logic Science

Instrument VMPX). The cell impedance was measured using a frequency analyzer (Solartron 1260) in the frequency range from 1 MHz to 0.1 Hz.

3. Results and Discussion

Figure 2 shows the evaporation rate of HAc-saturated LiAc aqueous solution (9:1 v/v) under 0.1 MPa and 0.2 MPa. The evaporation rate of 1.6×10^{-3} g cm^{-2} h^{-1} at 0.1 MPa is considerably suppressed to 5×10^{-4} g cm^{-2} h^{-1} at 0.2 MPa. An aqueous cathode can easily circulate in a flow through the configuration proposed by Goodenough and co-workers [14]. The system can individually store a large amount of cathode active materials in a fuel tank. The evaporation loss of the cathode active material for 1,000 h is around 0.5 g cm^{-2}. The capacity loss for 5 g of the cathode active material is around 10% for 1,000 h operation, which may be acceptable for a practical battery.

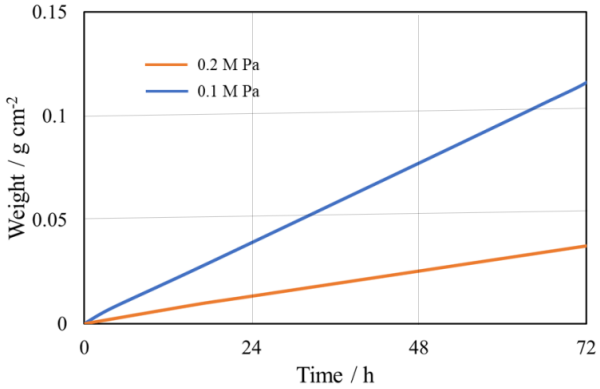

Figure 2 Weight loss of HAc-saturated LiAc aqueous solution (9:1 v/v) at 25 °C and 0.2 MPa and 0.1 MPa air with time. The flow rate of air was 80 mL min^{-1}.

The non-aqueous lithium-air battery shows high polarization for the oxygen reduction reaction (ORR) and oxygen evolution reaction (OER) [15]. To reduce the high polarization, a new concept of a highly soluble redox shuttle was proposed [16]; however, the reported current density of the cell was less than 0.5 mA cm^{-2} under pure oxygen. The aqueous lithium-air battery operates at a higher current density than that of the non-aqueous system. Minami et al. recently reported that an alkaline aqueous lithium-air cell of Li/4.5 M LiFSI in DME/LATP/1.5 M LiOH-10 M LiCl/$LiMnO_2$, the air was successfully cycled at 2.0 mA cm^{-2} and room temperature [7]. An ALAB of Li/(LiFSI-2 tetraethylene glycol dimethyl ether)-50 vol% 1,3 dioxolane/$Li_{1.4}Al_{0.4}Ge_{0.2}Ti_{1.4}(PO_4)_3$/HAc-saturated LiAc aqueous solution (9:1 v/v)/Pt-C-VGCF-PTFE, air was successfully cycled at 0.2 mA cm^{-2} and 25 °C [9]. In this study, the cell performance at a high pressure of 0.2 MPa was employed to reduce the evaporation of HAc and improve the cell performance at a high current density. Transition metal oxide-based catalysts cannot be used for the ALAB due to instability in the acid aqueous solutions. In this study, we have employed the platinum-loaded porous carbon air electrode used for fuel cells [17]. Figure 3 shows the polarization behavior of the Pt/C-VGCF (or KB)-PTFE composite electrodes for the ORR and OER at 25 °C and 0.2 MPa, where the overvoltage was measured after 1 h polarization at each current density. The lowest overvoltage was observed for the Pt/C-VGCF-PTFE (5:3:2 w/w) air electrode, which was used for the full cell performance test. Paganin et al. [18] reported that the NAFION loading in the catalyst layer of the air electrode for

polymer electrolyte membrane fuel cells improved the polarization behavior for the ORR. However, no significant improvement of the ORR and OER for the Pt/C-VGCF-PTFE air electrode in the acetic acid catholyte was observed by NAFION loading. Figure 4 compares the polarization behavior of the ORR and OER for Pt/C-VGCF-PTFE (5:3:2 w/w) at 0.1 and 0.2 MPa. The polarization of the ORR at 0.2 MPa was slightly improved compared with that at 0.1 MPa.

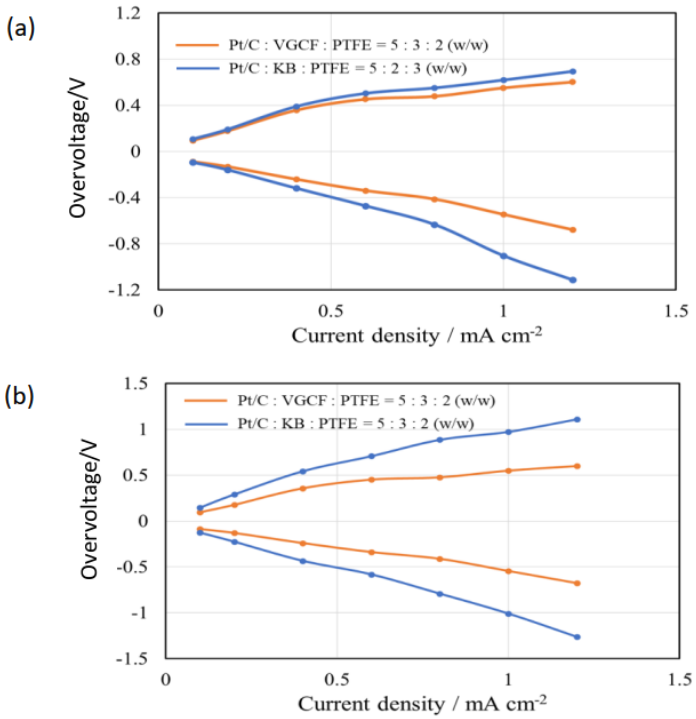

Figure 3 Overvoltages for the ORR and OER vs. current density curves for the mixture of Pt/C, VGCF (or KB), and PTFE air electrodes in HAc-saturated LiAc aqueous solution (9:1 v/v) at 25 °C and 0.2 MPa air. (a) Pt/C:VGCF:PTFE = 5:3:2 and Pt/C:KB:PTFE = 5:2:3, and (b) Pt/C:VGCF:PTFE = 5:3:2 and Pt/C:KB:PTFE = 5:3:2. The overvoltages were recorded after 1 h polarization.

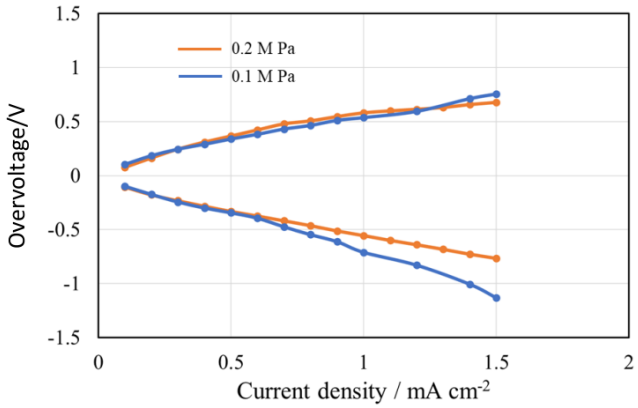

Figure 4 Overvoltages for the ORR and OER vs. current density curves at 25 °C for the mixture of Pt/C, VGCF, and PTFE (5:3:2 w/w) air electrodes in HAc-saturated LiAc aqueous solution (9:1 v/v) at 0.1 MPa and 0.2 MPa air. The over-voltages were recorded after 1 h polarization.

Figure 5 shows a cyclic voltammogram (CV) for the Pt/C-VGCF-PTFE (5:3:2 w/w) electrode in HAc-saturated LiAc aqueous solution (9:1 v/v) measured at a scan rate of 1.0 mV s^{-1} and 0.2 MPa. The CV result shows a trace oxidation current above 1.2 V vs. NHE. The calculated OER potential of the HAc-saturated LiAc aqueous solution (9:1 v/v) (pH = 2.7) at 0.2 MPa is 1.07 V vs. NHE. Wu et al. observed no oxidation of HAc in 0.25 M HAc + 0.5 M H_2SO_4 on a PtRuSn/C (60:30:10 w/w) electrode [19], which agreed with the results reported by Sine et al. [20]. Hence, the observed oxidation current in the CV curve is attributed to the OER.

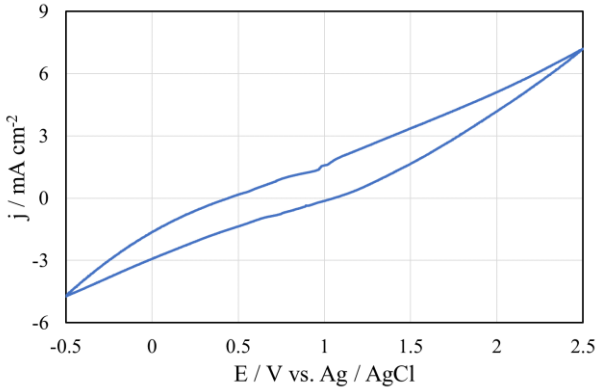

Figure 5 CVs measured at a scan rate of 1.0 mV s^{-1} for Pt/C-VGCF-PTFE (5:3:2 w/w) in HAc-saturated LiAc aqueous solution (9:1 v/v) at 25 °C and 0.2 MPa.

Figure 6 shows charge and discharge overvoltage vs. current density curves for the Li/1M LiFSI in DX-DME (1:2 v/v)/LATP/HAc-saturated LiAc aqueous solution (9:1 v/v)/Pt/C-VGCF-PTFE (5:3:2 w/w), air full cell at 0.2 MPa and 25 °C, where the airflow rate was 80 mL min^{-1}. The overvoltages after 1 h polarization at each current density are plotted. The open-circuit voltage (OCV) of 3.8 V is lower than the calculated OCV of 4.10 V using reaction (2) at a pH of 2.8 for the HAc-LiAc saturated aqueous solution (9:1) at 0.2 MPa. The low OCV may be due to the low activity of oxygen and lithium ions at the air and lithium electrodes, and the junction potentials between LATP and the liquid electrolytes. A discharge overvoltage of 0.58 V at 0.4 mA cm^{-2} corresponds to an approximate 15% energy loss of the discharge process.

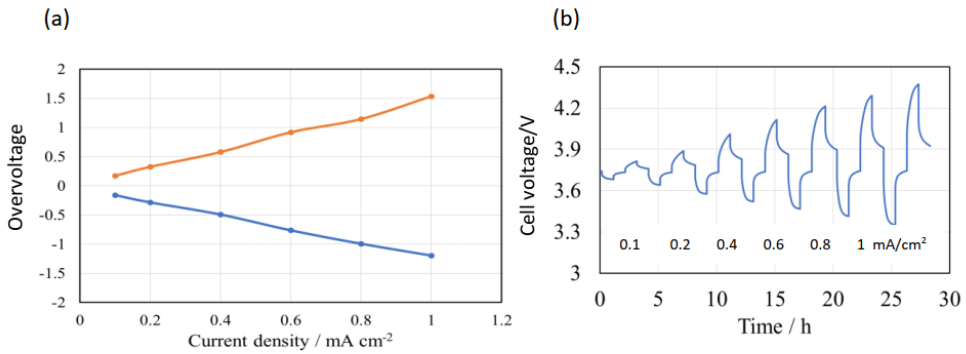

Figure 6 (a) Charge and discharge overvoltage vs. current density curves and (b) charge-discharge curves at various current densities for the Li/1 M LiFSI in DX-DME (1:2 v/v)/LATP/HAc-saturated LiAc aqueous solution (9:1 v/v)/Pt/C-VGCF-PTFE (5:3:2 w/w) cell at 25 °C and 0.2 MPa air. Overvoltages were recorded after 1 h polarization.

Figure 7 shows impedance profile of the Li/1M LiFSI in DX-DME (1:2 v/v)/LATP/HAc-saturated LiAc aqueous solution (9:1 v/v)/Pt/C-VGCF-PTFE (5:3:2 w/w), air full cell at 0.2 MPa and 25 °C. The impedance profile shows two semi-circles. The semi-circle in the high-frequency range of 1 M Hz to 13 k Hz can be assigned to be the grain boundary resistance of LATP (R_g) and the solid electrolyte interlayer resistance at the lithium anode; while the semi-circle in the low-frequency range of 13 k Hz to 3 Hz can be assigned to the charge transfer resistance (R_c). The contribution of the bulk resistance of LATP (R_b) was out of the frequency range of the analyzer [21]. The intercept of the high-frequency semi-circle with the real axis is the sum of R_b and the resistances of the liquid electrolytes of 1M LiFSI in DX-DME (1:2 v/v) (R_1) and the HAc-saturated LiAc aqueous solution (9:1 v/v) (R_2). The bulk and grain boundary resistances of the 0.25 mm thick LATP were 31 and 290 Ω cm^2, and the charge transfer resistance was 89 Ω cm^2. The main part of the total cell resistance of 725 Ω cm^2 is the resistance of the anolyte, catholyte, and bulk LATP (447 Ω cm^2). The electrical conductivities of the anolyte and the catholyte were 2×10^{-2} and 3×10^{-3} S cm^{-1}, respectively. The electrolyte volumes of the catholyte and anolyte in the Swagelok-type cell were approximately 1 mL, and the contact area with LATP was 1.13 cm^2. The estimated resistance of the catholyte and anolyte were 42 and 286 Ω cm^2, respectively. The sum of these resistances is 359 Ω cm^2. The estimated resistance of R_1+R_2 +R_g was slightly lower than the observed one. R_1 could be reduced considerably by the cell design, such as a laminate type, and R_2 could be reduced by the use of a catholyte flow system [14].

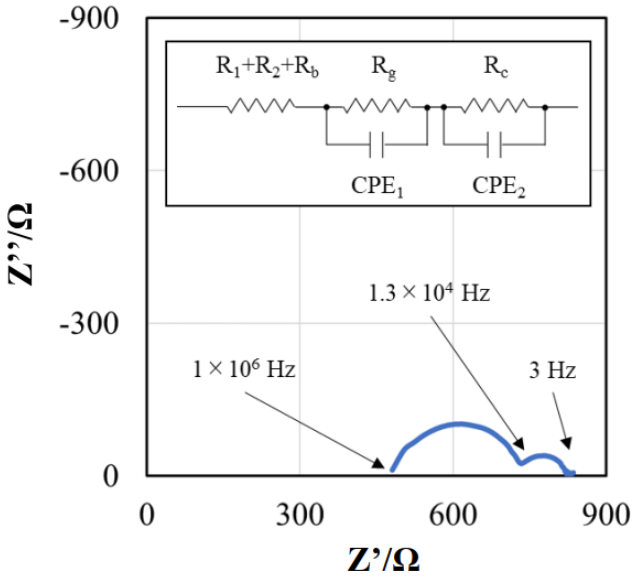

Figure 7 Cell impedance of Li/1 M LiFSI in DX-DME (1:2 v/v)/LATP/HAc-saturated LiAc aqueous solution (9:1 v/v)/Pt/C-VGCF-PTFE (5:3:2 w/w), air cell at 0.2 MPa and 25 °C.

The charge and discharge cycle performance of the Li/1 M LiFSI in DX-DME (1:2 v/v)/LATP/HAc-saturated LiAc aqueous solution (9:1 v/v) full cell at 0.2 MPa, 25 °C and 0.07 mA cm^{-2} for 5 h polarization (0.38 mAh) is shown in Figure 8. Excellent cycle performance at 0.07 mA cm^{-2} for more than 50 cycles was observed at 0.2 MPa and 25 °C under an air atmosphere. No carbon dioxide contamination was observed for more than 500 h, while the cell performance of an alkaline aqueous lithium-air cell degraded after 70 h operation in the air due to carbon dioxide

contamination [22]. The discharge overvoltage at 0.07 mA cm^{-2} was 0.2 V, which corresponds to an energy loss of around 5%.

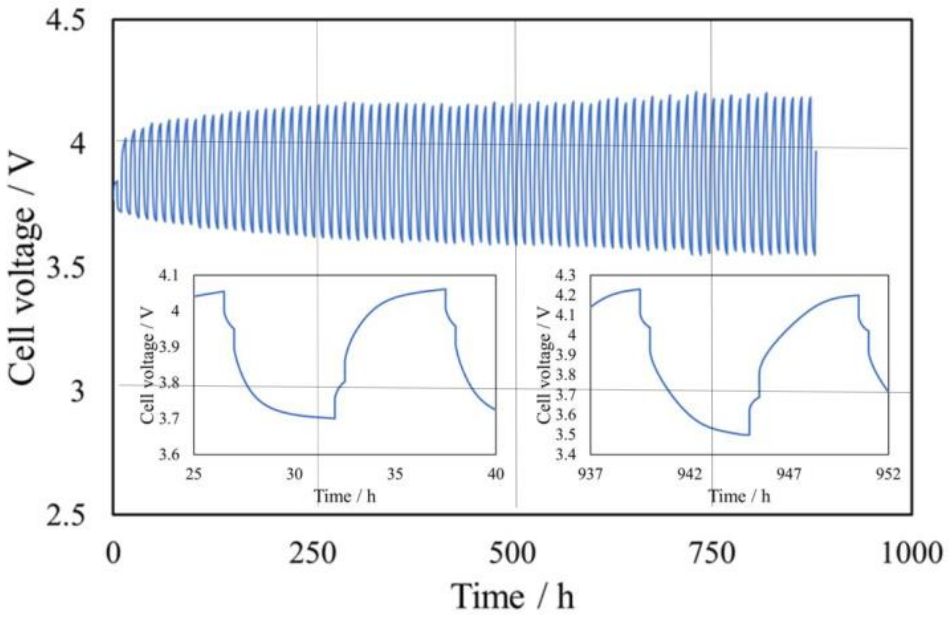

Figure 8 Cycle performance of the Li/1 M LiFSI in DX-DME (1:2 v/v)/LATP/HAc-LiAc saturated aqueous solution (9:1 v/v)/Pt/C-VGCF-PTFE (5:3:2 w/w) air cell at 0.07 mA cm^{-2} for 5 h at 25 °C and 0.2 MPa.

Figure 9 also shows the cycle performance at 0.2, 0.5, and 1.0 mA cm^{-2} for 5 h polarization and 0.2 MPa under air. Excellent cycle performance was observed at room temperature. The discharge overvoltage at 0.2 mA cm^{-2} was 0.27 V after the 1st cycle, which gradually increased by cycling to 0.3 V after 20 cycles. The overvoltage was steady with further cycling. The energy loss for the discharge process is around 8%. The initial discharge overvoltage of 0.58 V at 0.5 mA cm^{-2} gradually increased by cycling to 0.94 V after 20 cycles. With further cycles, the overvoltages were steady. At 1.0 mA cm^{-2} for 5 h polarization, the cell was successfully cycled for 20 cycles under air. The discharge overvoltage at 1.0 mA cm^{-2} was 1.0 V after the 1st cycle and 1.4 V after 20 cycles. The increase in the overvoltage by cycling may be due to degradation of the air electrode structure, as carbon particles were observed in the catholyte after the cycling tests – LiAc deposited in the air electrode may break the carbon-polymer network. The 1.4 V overvoltage corresponds to an energy loss of around 30%. The previously reported non-aqueous lithium-oxygen cells were operated at a lower current density [15]. Zhang et al. reported a high discharge overvoltage of a Li/0.5 M $Li(CF_3SO_2)_2N$-30 mM tetrathiafulvalene-50 mM LiCl in diethylene glycol dimethyl ether/graphene oxide, O_2 cell as 0.75 V at 0.2 mA cm^{-2} for 5 h polarization [23]. Bergner et al. reported the cell performance of a Li/10 mM TEMPO (2,2,6,6 tetramethylpiperdinyloxyl)-0.1 M $Li(CF_3SO_2)_2$ in diglyme/KB, O_2 cell – the discharge over-voltage at 0. 1 mA cm^{-2} was around 0.75 V after 50 cycles [24]. The discharge overvoltages of the ALABs are lower than those of the non-aqueous lithium-oxygen batteries. The discharge overvoltages for the ALABs may be reduced considerably by reducing the thickness of the liquid electrolytes because the bulk of the cell resistance is due to the liquid electrolyte resistances, as shown in Figure 7.

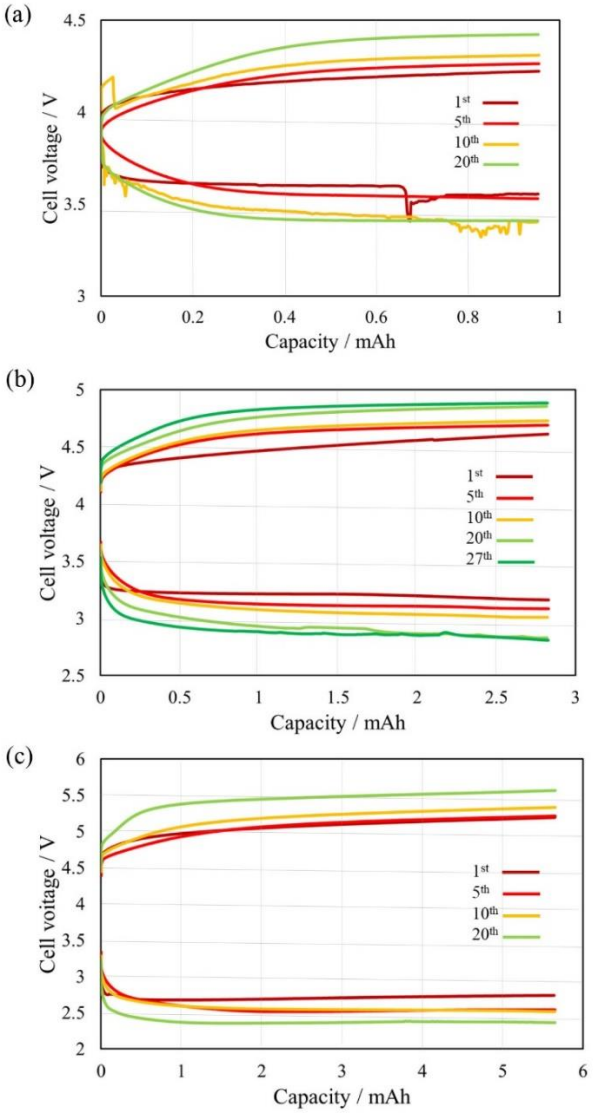

Figure 9 Cycle performance of the Li/1 M LiFSI in DX-DME (1:2 v/v)/LATP/HAc-LiAc saturated aqueous solution (9:1 v/v)/Pt/C-VGCF-PTFE (5:3:2 w/w), air cell at (a) 0.2 mA cm^{-2}, (b) 0.5 mA cm^{-2}, and (c) 1.0 mA cm^{-2} at 25 °C and 0.2 MPa.

4. Conclusion

The cell performance of the ALABs with acetic acid as the catholyte was studied at 0.2 MPa under an air atmosphere and room temperature. The evaporation of acetic acid was considerably reduced with operation at 0.2 MPa, and the cell was successfully operated at 0.5 mA cm^{-2} for 5 h polarization with 27 cycles in air. The ALABs showed no CO_2 contamination for 500 h operation. The steady discharge over-voltage at 0.5 mA cm^{-2} was around 1 V. The overvoltage for the charge, and discharge processes may be improved by reducing the thickness of the anolyte and catholyte.

Acknowledgments

This research was sponsored by a Grand in Aid for Scientific Research (20k05685) from the Mistry of Education, Culture, Sport, Science and Technology of Japan.

Author Contributions

S.H. investigation, formal analysis; D.M. S.T. and T. Z formal analysis, review & editing; Y.T. review & editing; O.Y. supervision, writing, review & editing; N.I supervision, project administration, review & editing.

Competing Interests

The authors have declared that no competing interests exist.

References

1. Tian Y, Zeng G, Rutt A, Shi T, Kim H, Wang J, et al. Promises and challenges of next-generation "Beyond Li-ion" batteries for electric vehicles and grid decarbonization. Chem Rev. 2020; 121: 1623-1669.
2. Grairee G. The coming electric vehicle transportation: A future electric transportation market will depend on battery innovation. Science. 2019; 366: 422-424.
3. Lu J, Li L, Park JB, Sun YK, Wu F, Amine K. Aprotic and aqueous Li-O_2 batteries. Chem Rev. 2014; 114: 5611-5640.
4. Manthiram A, Fu Y, Chung SH, Zu C, Su YS. Rechargeable lithium-sulfur batteries. Chem Rev. 2014; 114: 11751-11787.
5. Muldoon J, Bucur CB, Gregory T. Quest for nonaqueous multivalent secondary batteries: Magnesium and beyond. Chem Rev. 2014; 114: 11683-11720.
6. Chen R, Li Q, Yu Xiqian, Chen L, Li H. Approaching practically accessible solid-state batteries: Stability issues related to solid electrolyte and interface. Chem Rev. 2020; 120: 6820-6877.
7. Minami H, Izumi H, Hasegawa T, Bai F, Mori D, Taminato S, et al. Aqueous lithium--air batteries with high power density at room temperature under air atmosphere. J Energy Power Technol. 2021; 3. Doi: 10.21926/jept.2103041.
8. Zhang T, Imanishi N, Shimonishi Y, Hirano A, Takeda Y, Yamamoto O, et al. A noble high energy density rechargeable lithium/air battery. ChemComm. 2010; 46: 1661-1663.
9. Soga S, Bai F, Zhang T, Kakimoto K, Mori D, Taminato S, et al. Ambient air operation rechargeable lithium-air battery with acetic acid catholyte. J Electrochem Soc. 2020; 167: 090522.
10. Li L, Zhao X, Manthiram A. A dual-electrolyte rechargeable Li-air battery with phosphate buffer catholyte. Electrochem Commun. 2012; 14: 78-81.
11. Le HT, Ngo DT, Kim YJ, Park CN, Park CJ. A perovskite-structured aluminium-substituted lithium lanthanum titanate as a potential artificial solid-electrolyte interface for aqueous rechargeable lithium-metal-based batteries. Electrochim Acta. 2017; 248: 232-242.
12. Shimonishi Y, Zhang T, Johnson P, Imanishi N, Hirano A, Takeda Y, et al. A study on lithium/air secondary batteries-stability of NASICON-type glass ceramics in acid solutions. J Power Sources. 2010; 195: 6187-6191.
13. Miao R, Yang J, Xu Z, Wang J, Nuli Y, Sun L. A new ether-based electrolyte for dendrite-free lithium-metal based rechargeable batteries. Sci Rep. 2016; 6: 21771.
14. Lu Y, Goodenough JB, Kim Y. Aqueous cathode for next-generation alkali-ion batteries. J Am Chem Soc. 2011; 133: 5756-5759.

15. Imanishi N, Yamamoto O. Perspectives and challenges of rechargeable lithium-air batteries. Mater Today Adv. 2019; 4: 100031.
16. Chase CV, Zecevie S, Wesley TW, Uddin J, Sakai KA, Vincent PG, et al. Soluble oxygen evolution catalysts for rechargeable metal-air batteries. Washington: US Patent; 2012; US2012/0028137A1.
17. Litster G, McLean G. PEM fuel cell electrode. J Power Sources. 2004; 130: 61-76.
18. Paganin V, Ticianelli E, Gonzalez ER. Development and electrochemical studies of gas diffusion electrodes for polymer electrolyte fuel cells. J Appl Electrochem. 1996; 26: 297-304.
19. Wu G, Swaidan R, Cui G. Electrooxidations of ethanol, acetaldehyde and acetic acid using PtRuSn/C catalysts prepared by modified alcohol-reduction process. J Power Sources. 2007; 172: 180-188.
20. Siné G, Smida D, Limat M, Foti G, Comninellis C. Microemulsion synthesized Pt/Ru/Sn nanoparticles on BDD for alcohol electro-oxidation. J Electrochem Soc. 2006; 154: B170.
21. Bruce PG, West AR. The AC conductivity of polycrystalline LISICON $Li_{2+2x}Zn_{1-x}GeO_4$ and a model of intergranular constriction resistance. J Electrochem Soc. 1983; 130: 662-669.
22. Sunahiro S, Matsui M, Takeda Y, Yamamoto O, Imanishi N. Rechargeable aqueous-air batteries with an auxiliary electrode for the oxygen evolution. J Power Sources. 2014; 262: 338-343.
23. Zhang J, Sun B, Zhao Y, Kretschmer K, Wang G. Modified tetrathiafulvalene as an organic conductor for improving performance of Li-O_2 batteries. Angew Chem Int Ed. 2017; 56: 8505-8509.
24. Bergner BJ, Schirman A, Peppler K, Garsucjh A, Janek J. TEMPO: A mobile catalyst for rechargeable Li-O_2 batteries. J Am Chem Soc. 2014; 136: 15054-15064.